ORIGINAL PAPER

Decadal oscillations in rainfall and air temperature in the Paute River Basin—Southern Andes of Ecuador

D. E. Mora · P. Willems

Abstract In the Andes environment, rainfall and temperature can be extremely variable in space and time. The determination of climate variability and climate change needs a special assessment for water management. This paper examines the anomalies of observed monthly rainfall and temperature data from 25 to 16 stations, respectively, from the early 1960s to the 1990s. The stations are located in the Rio Paute Basin in the Ecuador's Southern Andes. All stations are within the elevation band 1,800 and 4,200 m a.s.l. and affected by the Tropical Pacific, Amazon, and Tropical Atlantic climate. Anomalies in quantiles were determined for each station and their significance tested. In addition, their correlations with different external climatic influences were studied for anomalies in annual and 3-month seasonal block periods. The results show similar temperature variations for the entire region, which are highly influenced by the El Niño–Southern Oscillation, especially during the December–February season. During June–August, the correlation is weaker showing the influence of other climate factors. Higher temperature anomalies are found at the high elevation sites while at deep valley sites the anomalies are less significant. Rainfall variations depend, in addition to elevation, on additional factors such as the aspect orientation, slope, and hydrological regime. The highest and most significant rainfall anomalies are found in the eastern sites.

D. E. Mora (✉) · P. Willems
Hydraulics Division, Katholieke Universiteit Leuven,
Kasteelpark Arenberg 40,
3001 Heverlee, Belgium
e-mail: diego.moraserrano@bwk.kuleuven.be

D. E. Mora
Universidad de Cuenca,
Av. 12 de abril,
Cuenca, Ecuador

P. Willems
Department of Hydrology & Hydraulic Engineering,
Vrije Universiteit Brussel,
Pleinlaan 2,
1050 Brussels, Belgium

1 Introduction

Climatic variability and change play an important role in economic and social decisions made by governmental bodies. According to the fourth Intergovernmental Panel on Climate Change report, the main impacts for the tropical Andes region are a clear increase in mean surface temperature (Solomon et al. 2007), disappearance of glaciers in Colombia, Ecuador, Peru, and Bolivia caused by changes in temperature and humidity (Vuille et al. 2008), higher variability in the extreme events of rainfall (Parry et al. 2007; Ontaneda et al. 2002), and decreasing rainfall depths for the Amazon Basin (Villar et al. 2009). Ecosystems may suffer drastic impacts, as a result of longer drought periods and higher intensity rainfalls that could cause more frequent floods (Parry et al. 2007; Buytaert et al. 2010).

In this context, determination of the main climate trends in the region is required in support of the design of mitigation and/or adaptation actions and to increase our knowledge toward higher quality future climate projections. The Andes region in the Amazon Basin, including the South Ecuadorian Andes, shows the highest weather and climate variability (Villar et al. 2009). Due to this high heterogeneity in climate, it is important to understand the drivers that influence the climate at small scale in this region and that could be related to the variations and trends observed in local weather stations.

The tropical region in northwest South America is climate-dominated by convergence zones such as the

Inter-tropical Convergence Zone (ITCZ), the South Atlantic Convergence Zone, and therefore with other climate anomalies as the South America Monsoon System and the El Niño Southern Oscillation (ENSO). Linked to the ENSO, strong positive sea surface temperature anomalies along the coast of Ecuador and northern Peru bring torrential rains, high river runoff, and flooding, additional to an intensification of the ITCZ over the eastern Pacific. These periods are called El Niño events. Strong negative sea surface temperature anomalies, La Niña events, bring low temperatures, dry seasons, and stress in water availability. However, effects of ENSO could lead to different weather behaviors in the Andes region; hence, there is the need for further research in this region.

The ENSO is one of the main climate anomalies that drive the region, including the Andean region. Marengo (2009) indicated that ENSO variability was detected in rainfall in the northern Amazon with a low-frequency variability. This leaves the uncertainty that ENSO might cross the Andes with a lower magnitude influence too. However, he also indicated that multi-decadal variations of rainfall in the Amazon might be linked to sea surface temperatures (SSTs) in the subtropical Atlantic. Meanwhile, Francou et al. (2004) indicated a strong dependence of ENSO on the Antizana mountain ablation–snowfall in the north of Ecuador.

Bendix and Bendix (2006) investigated the dynamics of heavy rainfall during El Niño events in the coastal area of Ecuador and northern Peru. Their study developed 16 factors each one with different specific weather situations that could lead to moist instability and heavy rainfall during El Niño events. Three of their factors, which explain nearly half of the total rainfall variance, are linked to well-developed rainfall in the Amazon region crossing the Andes over the Ecuador region and that ends in heavy rainfall in the coastal region. Hence, heavy rainfall during El Niño events, according to these factors, can originate from weather patterns that are also relevant in non-El Niño periods. We learn from that research that, although a moderate positive SST anomaly off the coast causes an intensification of rainfall in the coastal area of Ecuador and northern Peru during El Nino, it is not the only factor that controls rainfall extremes. Wang and Fiedler (2006) indicated that ENSO variability is most pronounced along the equator and the coast of Ecuador and Peru, developing strong or weak ENSO events. This variation might be caused by westerly wind anomalies produced in the equatorial western Pacific and precedes the Nino3 SST anomalies by about 4 months. It suggests that the western Pacific is an important region for defining the ENSO variability and its influence on the coast of Ecuador and Peru.

The effects of the ENSO and the ITCZ anomalies are highly visible in the Coastal Pacific region, but the effects are less clear and little is known about the influence of factors inland through the Andes Mountains. The high heterogeneity of climate variables in that inland region, for both rainfall and temperature, is one of the reasons.

Vuille et al. (2000) took different weather stations along the Ecuadorian Andes and found that the rainfall variability in the Andes area of Ecuador is related to the sea surface temperature anomalies in the Pacific. They also found that this ENSO influence is most dominant in the region during December–February (DJF) and also strongly influences the Eastern Cordillera (Real Cordillera) during June–August (JJA). In both cases, below or above average rainfall is associated with El Niño or La Niña events, respectively (inverse of what occurs along the coastal front). They additionally concluded that the weather in the Eastern Cordillera in the other periods of the year is correlated to the ITCZ in the tropical South Atlantic, and in few local areas in the south of the Eastern Cordillera between 1° and 3° S, the weather is correlated with the El Nino events in the period DJF. The study of Vuille et al. (2000) also concluded that temperature along the Ecuadorian Andes is largely correlated to sea surface temperature anomalies in the Tropical Pacific domain, following the response of ENSO Region 3 (5° N–5° S, 150° W–90° W) and ENSO Region 3.4 (5° N–5° S, 170° W–120° W). They additionally noticed that the weather in the Northern Cordillera is correlated with the Tropical North Atlantic sea surface temperature anomaly.

Taking this prior knowledge into account, this paper aims to explain historical variations in rainfall and temperature by means of the main external influences (teleconnections) for one of the river basins in the Southern Ecuadorian Andes, the Paute River Basin. This is done based on several observed local weather stations distributed along the basin, estimation of the decadal oscillations or anomalies, and testing of their significance for periods of 30 years. It is studied how the rainfall and temperature oscillations are related to oscillations of the external climate variables. These relationships might enable us to determine future behaviors in the climate change context, as more knowledge (both in term of recent monitoring data and future scenario analysis) is available for these external climate variables.

The study makes use of the rainfall subregions that were identified for the Paute River Basin by Celleri et al. (2007) (see Fig. 1). They identified the subregions based on inter-station correlation analysis in two steps: the analysis of distribution of mean monthly precipitation to classify rainfall stations following contrasting rainfall regimes and monthly time series analysis in an attempt to identify secondary rainfall patterns. That study resulted in four different rainfall regimes, based on the annual distribution of rain: an Andean inter-valley regime (BM1), a high páramo mountain regime (BM2), a medium Amazon inter-valley regime (UM1), and a stronger Amazon inter-valley regime (UM2).
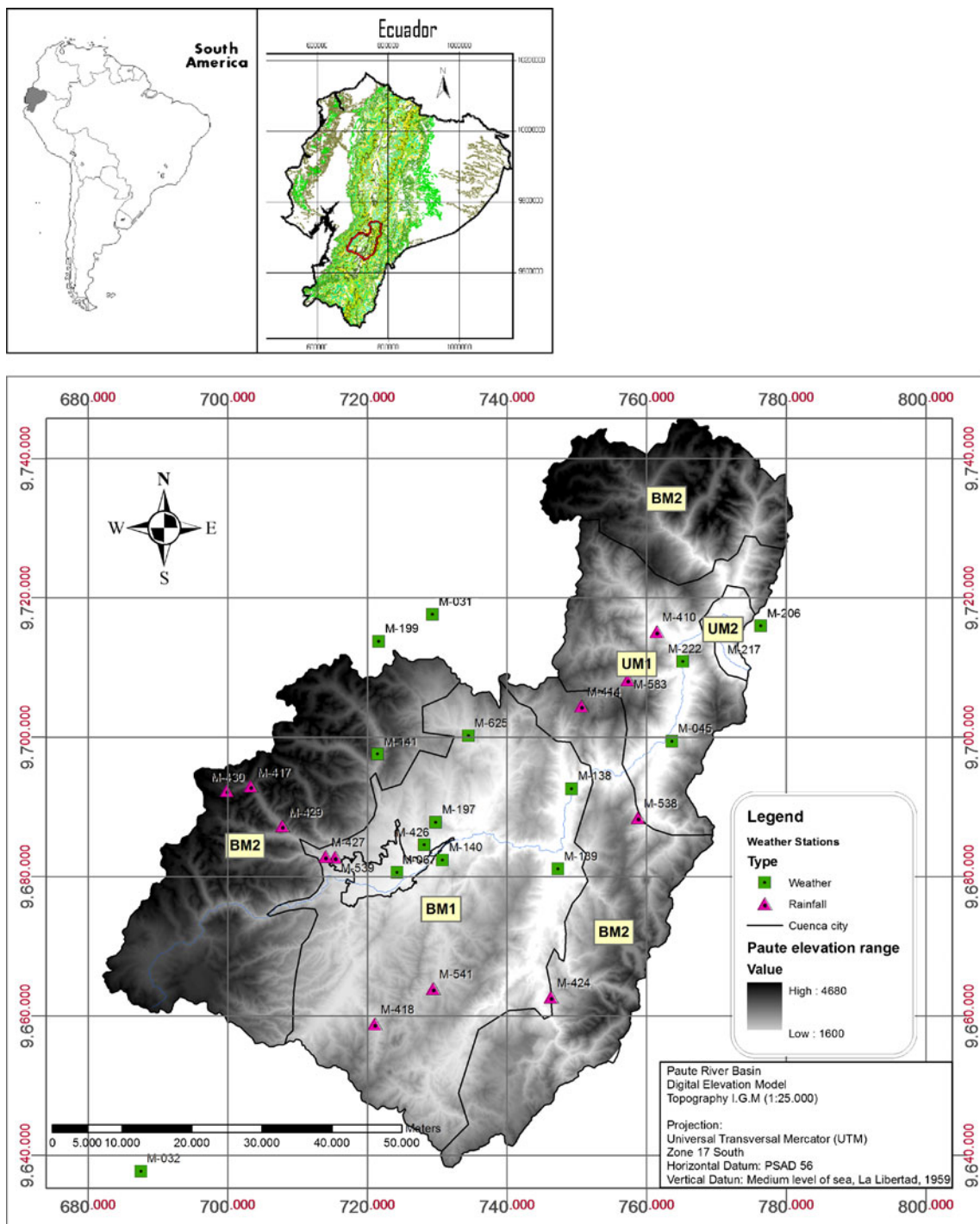
Fig. 1 Location of the Paute River Basin—weather and rainfall stations

In the next section, the data and the applied methodology are described. This is followed by a section that presents and discusses the results of the temporal variations, as well as the correlation with the main large-scale climate influences, for all the seasons and for 3-month seasonal periods. The final section summarizes the conclusions of this research and ends with some concluding remarks.

2 Methodology

2.1 Study region

The Paute River Basin is located in the Inter-Andean Depression that separates the Western and Real Cordillera in the south of Ecuador (Coltorti and Ollier 2000). The

basin has an area of 5,066 km^2 up to an important hydropower plant. The elevation range is from 1,840 to 4,680 ma.s.l. The upper part of the basin is located only 17 km from the Pacific coastal plains and 62 km from the Pacific coast line in its western point and the downstream part ends in the interspersed region between the Andes and the Amazon regions.

2.2 Data and filling gaps

The Paute River Basin is one of the most monitored basins in Ecuador since 1963 due to its importance in hydropower energy production. The monitoring data are dispersed in several databases ruled by different institutions: Instituto Nacional de Meteorología e Hidrología (INAMHI), Instituto Ecuatoriano de Recursos Hídricos (INERHI), and Instituto Ecuatoriano de Electrificación (INECEL). In 1987, the "Plan Nacional de Riego" project INERHI-ORSTOM (Office de la Recherche Scientifique et Technique d'Outre-Mer, France) developed a complete assessment of the existing data bases, including the revision on the quality of the data and merged the different databases in one database called BIDRIE (Le Goulven et al. 1987). Unfortunately, monitoring was canceled for most of the stations at the beginning of the 1990s due to the change of structure of governmental institutions (Galarraga-Sanchez 2000). The monitoring continued only in few sites. However, local institutions have monitored additional data in an independent way. Recent data are available at ETAPA (the drinking water authority for the city of Cuenca) for the period 1997–2004. These data, however, focus only in the western central region of the basin and lack spatial representation for the complete basin. In addition, INAMHI continued its monitoring only in two stations in the eastern region of the basin close to the hydropower station. Since 1993, the Paute River Basin has less well-distributed rainfall stations which could represent the rainfall regimes of the complete basin. The INAMHI administers today the hydrometeorological network of the country. For this research, data were compiled from the BIDRIE, INAMHI, and ETAPA databases, resulting in 25 rainfall stations, 11 started in 1962–1964, and 14 in 1972–75 till 1992–1993, from which three with recent data from 1997 to 2004 and 17 weather stations starting around 1958–1962 till 1990–1992. Figure 1 and Table 1 give an overview of the stations considered.

Data on regional weather patterns (climate external influences) are available in several climate databases as the ones of the National Oceanic and Atmospheric Administration (NOAA) and ERA40 or ERA Interim. For this study, climate indices of NOAA were used. This includes data on ENSO anomalies in SST, for ENSO 1.2, ENSO 3, ENSO 3.4 regions, and sea level pressure (SLP) at the Darwin–Tahiti station which reproduce the South Oscillation Index. Additionally, data corresponding to SST of the tropical South Atlantic (SST TSA), the Tropical Pacific Oscillation, and the Eastern Pacific Oscillation (SST EPO) are also considered. Also northeast Brazil rainfall data were included, with data from a rain gauge in Fortaleza (3.7 S, 38.5 W) in the Brazilian northeastern coast which might be under strong tropical South Atlantic influence. The length of these climate records might differ. For this study, data covering the period 1950–2005 were selected.

Missing periods in the observed rainfall and temperature series were filled by means of multiple linear regressions (Carter and Benson 1970; Makhuvha et al. 1997). The method first applies a logarithmic transformation to the data and then converts the data to normalized standard variables. Based on the converted data, correlation coefficients are calculated between all pairs of stations, for each current and preceding month, and applied in the multiple linear regression equation. In order to maintain a reasonable number of correlation coefficients, stations are first ranked by rainfall regime (Celleri et al. 2007; Torres 2004) and grouped in sets of six. In this way, the number of correlation coefficients is limited to 12: six from stations in the current month and six from the previous month. The number of coefficients is constant for all infillings. In a preview study, Villazon and Willems (2010) compared the multiple linear regression approach with the more classical linear regression technique for gap filling of rainfall series in Bolivia and found an important reduction in the daily rainfall error (36%) using the multiple linear regression technique.

2.3 Trends and anomalies

To study the recent trends in rainfall and temperature, it is necessary to understand the historical variations in these series. Based on these variations, which reflect the natural temporal variability, it can be tested whether the recent trends are statistically significant.

2.3.1 Quantile perturbation approach

Ntegeka and Willems (2008) proposed a methodology for the analysis of trends and anomalies in hydroclimatic extremes based on quantile perturbations. The perturbations refer to relative changes between two series. One of the series is taken as reference or baseline series while the other is a subseries of interest. In this study, the reference series are taken as the full available historical series, while the subseries are block periods of interest (i.e., 10 years). The quantile perturbation approach is applied to monthly series of rainfall and average temperature.

The monthly values within a subseries (particular block of L years) are ranked in descending order, where i is the

Table 1 Temperature and rainfall stations in the Paute River Basin

Temperature stations (monthly data)						Rainfall stations (monthly data)					
Station code	Station name	Elevation (m a.s.l.)	Aspect	Year average (°C)		Station code	Station name	Rainfall regime	Elevation (m a.s.l.)	Aspect	Year average (mm)
M199	PATOCOCHA	3,401	Northwest	8.2		M625	BIBLIAN	BM1	2,640	East	852.4
M141	EL LABRADO	3,260	South	8.4		M541	COCHAPAMBA QUINJEO	BM1	2,760	Northeast	816
M031	CANAR	3,083	East	11		M197	JACARIN	BM1	2,700	Northeast	719.5
M197	JACARIN	2,700	Northeast	14		M139	GUALACEO	BM1	2,360	Flat north	729.4
M625	BIBLIAN INECEL	2,640	East	13.6		M140	UCUBAMBA	BM1	2,510	Flat north	918.5
M426	RICAURTE CUENCA	2,545	Flat south	14.8		M418	CUMBE	BM1	2,720	Northwest	681.4
M067	CUENCA AEROPUERTO	2,516	Flat	14.7		M067	CUENCA AEROPUERTO	BM1	2,516	Flat south	846.2
M140	UCUBAMBA	2,430	Flat north	15.7		M426	RICAURTE CUENCA	BM1	2,545	Flat south	894.6
M045	PALMAS	2,400	Northwest	14.8		M138	PAUTE	BM1	2,289	Flat south	735.8
M139	GUALACEO	2,360	Flat north	17.1		M539	BUENOS AIRES AZUAY	BM1	2,810	South	843.6
M222	INGPATA	2,360	Northwest	14.6		M420	NABON	BM1	2,750	South	786.9
M138	PAUTE	2,289	Flat south	17.3		M427	SAYAUSI	BM1	2,780	Southeast	988.1
M050	ARENALES	2,200	East	14.1		M414	CHANIN	BM2	3,020	East	1,702.2
M217	PENAS COLORADAS	2,000	East	14.1		M424	SIGSIG	BM2	2,600	North	753
M206	GUARUMALES	1,645	Southeast	17.2		M141	EL LABRADO	BM2	3,260	South	1,280.5
M032	SANTA ISABEL	1,550	Southwest	19.2		M430	QUINOAS	BM2	3,200	Southeast	948.9
						M417	PISCICOLA CHIRIMICHAY	BM2	3,270	Southeast	1,256.7
						M429	SURUCUCHO (LLULLUCHAS)	BM2	2,800	Southeast	873.4
						M583	PINDILIG	UM1	2,700	East	1,076.2
						M410	RIO MAZAR-RIVERA	UM1	2,450	East	1,305.7
						M538	PANGRANDE	UM1	2,600	Northeast	1,094.6
						M222	INGPATA	UM1	2,360	Northwest	1,321.6
						M050	ARENALES	UM2	2,200	East	3,504.9
						M217	PENAS COLORADAS	UM2	2,000	East	3,076.1
						M045	PALMAS	UM2	2,400	Northwest	1,587.5

rank of a given month in the series. Based on this rank, the empirical return period $T_{L(i)}$ can be estimated according to Eq. 1 for each month in the subseries. The same calculations are applied to the full long-term series (Nyears), Eq. 2.

$$T_{L(i)} = \frac{L}{i} \qquad (1)$$

$$T_{N(i)} = \frac{N}{i} \qquad (2)$$

The monthly values that correspond to these return periods are denoted as the quantiles x_L, $x_{L/2}$,…,$x_{L/i}$ for the subseries and x_N, $x_{N/2}$,…$x_{N/i}$ for the full series. The perturbation factor $P_{(i)}$ for a given return period then corresponds to the ratio indicated in Eq. 3.

$$P_{(i)} = \frac{x_L\left(T_{L(i)}\right)}{x_N\left(T_{N(i)}\right)} \qquad (3)$$

It is clear that the empirical return periods $T_{L(i)}$ of the subseries do not necessarily coincide with the empirical return periods of the full series $T_{N(i)}$. In that case, the $x_N(T_{L(i)})$ values are derived by linear interpolation from the values with closest empirical return periods. From the perturbation factors of all months, an average perturbation factor can be calculated for all quantiles above a given threshold (or a given threshold for the return period, i.e., an empirical return period of 0.33 year). These average perturbation factors represent anomalies in quantiles and are calculated in this paper for moving block periods (subseries of 10 years length, moved with 1-year step from the beginning, toward the end of the full available series).

For a full series of Nyears [0;N], the following moving 10-year subseries thus are considered: [0;10], [1;11], …, [N–9;N]. The moving procedure causes dependency among the calculated anomalies (over periods of 10 years length) but allows easier visual interpretation of the temporal variations in these anomalies. The method allows to detect decadal and multi-decadal oscillations in extreme quantile anomalies (Ntegeka and Willems 2008).

The same procedure is applied but limiting the return period and perturbation factor calculations to a given season (i.e., December–January–February, March–April–May (MAM), June–July–August, September–October–November (SON)). In this case, the particular block period (subseries) of interest will be limited to the months in the given season.

2.3.2 Significance testing

Confidence intervals are calculated on the perturbation factors, under the null hypothesis of no trend or serial dependence in the occurrence of rainfall or temperature extremes in time. This is done to test whether the trends and anomalies identified in the historical series are significant.

The confidence intervals are calculated by a non-parametric bootstrapping technique. The values in the full series are randomly resampled a large number of times (1,000 bootstrap runs; each run containing the same number of values as in the full series) without replacement. For each run, perturbation factors are recomputed, where after confidence intervals are calculated for each time step based on the ranked 1,000 perturbation factors per time step.

Since these confidence intervals define regions of expected variability under the null hypothesis, any anomaly value outside the confidence bounds is considered to be statistically significant (hypothesis of no trend or serial dependence is rejected), while the region inside the confidence bounds is considered insignificant (hypothesis accepted; see Fig. 2).

2.3.3 Correlation

After determination of the anomalies for each of the stations, in both monthly rainfall and average temperature, together with the confidence intervals, comparison is made with the anomalies calculated in a similar way with data corresponding to regional climate influences as ENSO and ITCZ in the Pacific and the Atlantic. The aim of this comparison is to identify the external influences of the anomalies in rainfall and temperature. Sites with similar correlations are grouped to obtain regionalized estimates of the external influences.

The quantile perturbation approach was compared with a simple regression after logarithmic transformation. Results show that correlation values are about two times higher when the quantile perturbation method is used, i.e., correlation coefficients between monthly rainfall at station M538 versus SST ENSO1.2 and SST TSA equal −0.77 and 0.65 using the quantile perturbation approach, while the direct regression with logarithmic transformation results in correlation coefficients of −0.39 and 0.31, respectively. This is because the quantile perturbation method filters out information on the statistical frequency properties of the variables under study, which may lead to more clear teleconnection results (Ntegeka and Willems 2008).

3 Results

3.1 All-season anomalies

The results on SST ENSO anomalies show inter-annual oscillations from about 12–14 years with significant anomalies for the periods 1963–1968 (low anomaly), 1982–1984, 1992–1996 (high anomaly). Torrence and Webster (1999)

Fig. 2 Quantile perturbation analysis results for temperature and 95% confidence intervals on the perturbation factors: all seasons. All perturbation factors are in percent
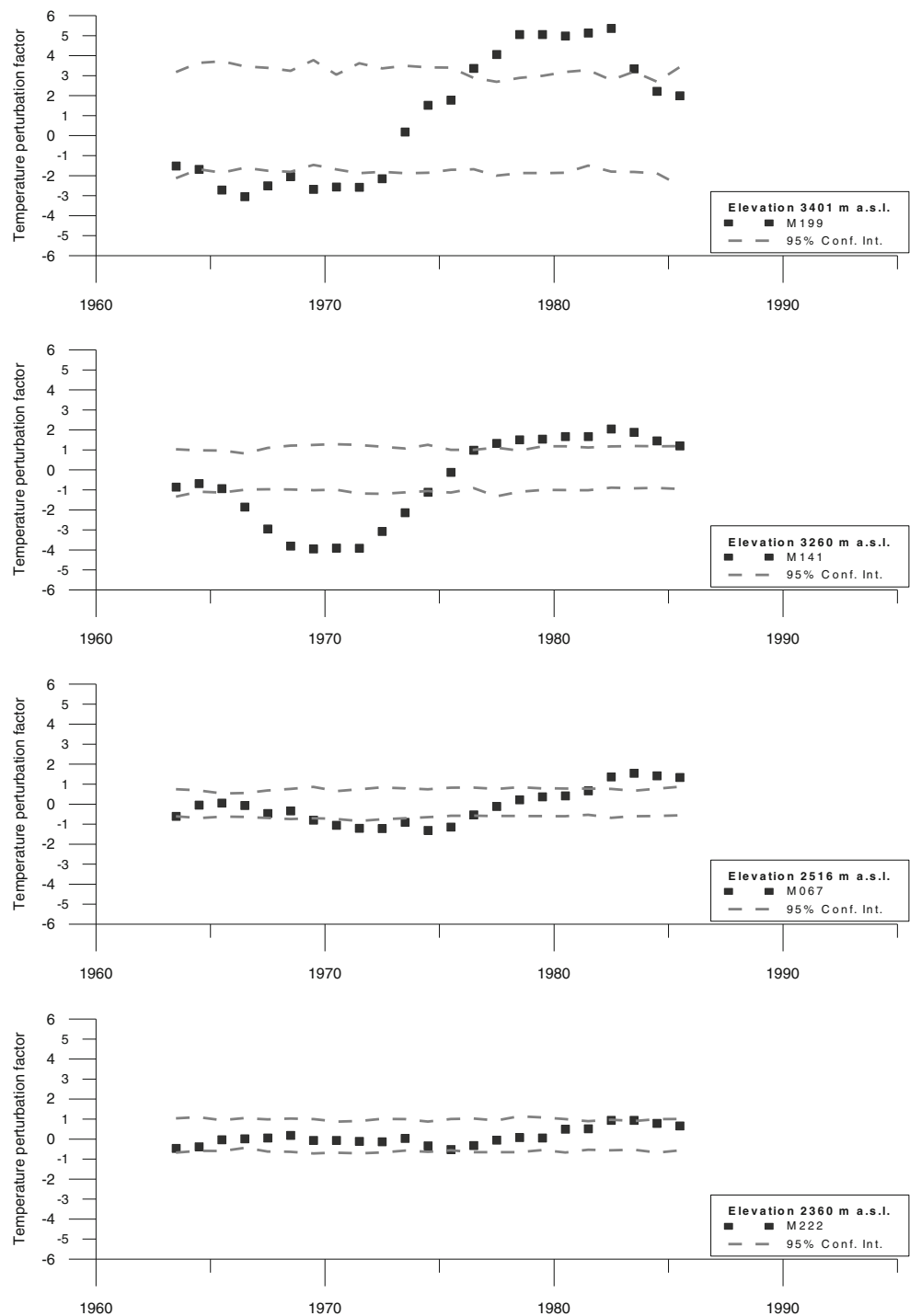
also found a 12–20-year oscillation period from 1875 to 1920 and 1960 to 1990. The SST TSA and Brazil rainfall anomalies show decadal–multi-decadal oscillations with low significance in anomalies except a few events that are related to ENSO. As the Brazil rainfall station might be located under tropical South Atlantic influence, the timing of the rainfall oscillations is similar with the SST TSA. Their correlation values, however, differ from each other.

3.1.1 Temperature

Results of anomalies in monthly temperature considering all seasons show that 13 out of the 16 stations present similar oscillations but differ in anomaly scale. Stations located at higher elevations (M199, M141, M031) show higher and more significant values of anomalies than the stations which are located in the inter-valley region (M426,

M222, M217, M067), which present low and less significant anomalies. The oscillations show a lower temperature period during 1968–1973 and a warmer period during 1978–1984 (Fig. 3).

The significance test applied to these anomalies shows that the oscillation highs and lows overpass the significance range more in sites located at high elevation than in the valleys. The anomaly values at the high elevations sites are two to five times higher. This means that the periods of high and low temperatures are more significant for higher elevation sites. Lower elevation sites show less significant anomaly values during these periods, with some exceptions (M138 and M050 at 2,289 and 2,200 ma.s.l., respectively). This is assumed to be the effect of orographic and topographic influences that create microclimates in the deep inter-valley region (Fig. 2).

The temperature anomaly patterns at the 13 stations have high correlation with the anomaly patterns of the SST ENSO 1.2 (Pacific coast of Ecuador) and ENSO 3 ($R^2 = 0.61$ and $R^2 = 0.64$, respectively; considering the average correlation of all 13 stations). For some stations, higher correlations are found. For the other three stations (M206, M139, M625), the correlation values show different behavior; small correlations are found with the ENSO and no correlation with the other climate external influences.

Given that the data record of SST ENSO anomalies is longer than the observed temperature records, the strong correlation with the temperature values allows to extrapolate the temperature series. Based on that extrapolation, high temperature anomalies are found in the mid-1990s and the beginning of the 2000s. A significant decrease is found in the beginning of the 1990s and the mid-2000s (Fig. 3). These oscillations could imply similar behavior to the local observed sites for future events, which needs to be confirmed. The correlation values are shown in Table 2.

The influence of SST ENSO1.2 on temperature is nearly homogeneous over the basin (Fig. 5), apart from the stations M625 and M139. The results at these two stations differ from the other stations, which might be due to a microclimate caused by terrain and orographic influences. It is also observed that the SST TSA is inversely correlated to the SST

ENSO1.2 and the Brazil rainfall along the basin, resulting in a similar homogeneous influence on temperature.

We learn from the temperature results that the River Paute Basin is largely correlated to sea surface temperature anomalies following ENSO variability and that the period where its influences are stronger is on DJF. Similar results were found by Vuille et al. (2000). Francou et al. (2004) also found that evolution of the Andes glaciers and temperature is positively correlated with ENSO variability for this region. The temperature influence of ENSO in the Andes region might be similar to the influence of ENSO in the Pacific coast region as was stated by Marengo (2009).

3.1.2 Rainfall

The results on the anomalies in rainfall are more complex than those for temperature. Stations with rainfall regimes corresponding to eastern sites (UM1 and UM2) have similar behavior, driven mainly by an inverse correlation with ENSO. Meanwhile, stations located in the inter-Andean valley and the high mountainous (páramo) regions (BM1 and BM2) show more heterogeneous behavior. This is due to additional influencing factors such as the location in the catchment, the rainfall regime, the topographical elevation, and the orientation of its slope (aspect). However, when the BM1 and BM2 stations are grouped according to their orientation (aspect), more similar results are found. In the inter-Andean valley regime (BM1), the stations show similar anomaly patterns for the stations with northeast versus southwest aspect. Same conclusion holds for the high mountain (páramo) regime (BM2).

A first group of 13 of the 25 stations shows similar anomaly patterns driven by inverse influence of ENSO. They are located in the downstream eastern part of the basin (UM1 and UM2 rainfall regimes) and at inter-Andean valley sites with a northeast aspect corresponding to the BM1 and BM2 rainfall regimes. High anomalies are observed for these stations during 1969–1974 and low anomalies during 1983–1986 (Fig. 4a, b).

Another group of nine stations, mainly located in the inter-Andean valley regions with southwest aspect, shows high anomalies during 1978–1981, 1986–1989, and 1996–

Fig. 3 Temperature and ENSO SST quantile perturbation analysis results: all seasons. All perturbation factors are in percent
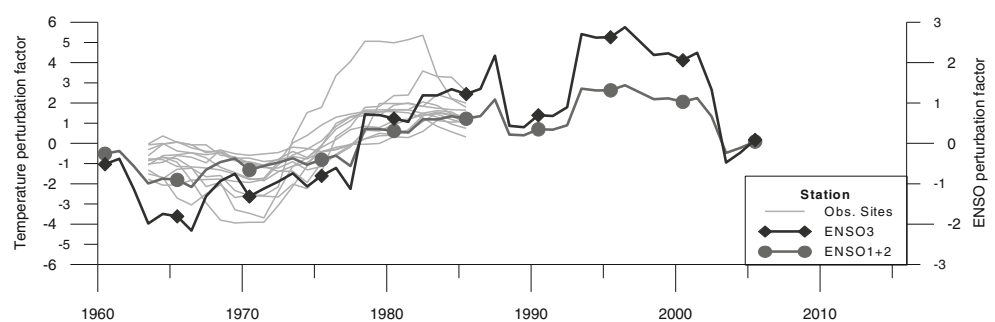
Table 2 Correlation in temperature and rainfall perturbation factor vs large-scale climate influences: all seasons

Temperature

Station code	Large-scale climate influence						
	SST ENSO 1 + 2	SST ENSO 3	SST ENSO 3.4	SLP D-T	Brazil rainfall	Eastern Pacific	SST TSA
M199	0.77	0.71	0.44	-0.41	0.91	0.00	-0.59
M141	0.69	0.67	0.47	-0.62	0.76	-0.30	-0.69
M031	0.78	0.78	0.64	-0.72	0.68	-0.43	-0.61
M197	0.70	0.70	0.52	-0.68	0.74	-0.32	-0.77
M625	-0.63	-0.67	-0.69	0.84	-0.39	0.67	0.52
M426	0.79	0.85	0.84	-0.77	0.56	-0.62	-0.50
M067	0.75	0.83	0.87	-0.80	0.50	-0.69	-0.50
M140	0.68	0.61	0.32	-0.36	0.87	0.05	-0.59
M045	0.88	0.90	0.75	-0.61	0.83	-0.33	-0.53
M139	0.04	0.01	0.01	0.44	0.01	0.44	0.66
M222	0.80	0.89	0.93	-0.63	0.52	-0.54	-0.19
M138	0.87	0.82	0.59	-0.44	0.91	-0.13	-0.49
M050	0.87	0.89	0.79	-0.71	0.77	-0.45	-0.59
M217	0.91	0.90	0.82	-0.44	0.71	-0.34	-0.18
M206	0.26	0.11	-0.23	0.21	0.58	0.53	-0.18
M032	0.69	0.78	0.82	-0.87	0.45	-0.71	-0.62

Rainfall

Station code	Large-scale climate influence						
	SST ENSO 1 + 2	SST ENSO 3	SST ENSO 3.4	SLP D-T	Brazil rainfall	Eastern Pacific	SST TSA
BM1							
M625	-0.56	-0.55	-0.44	0.67	-0.71	0.27	0.62
M541	-0.50	-0.50	-0.33	0.71	-0.82	0.23	0.68
M197	-0.63	-0.66	-0.58	0.90	-0.69	0.39	0.47
M139	-0.76	-0.76	-0.70	0.73	-0.50	0.59	0.58
M140	0.43	0.37	0.29	0.25	-0.73	0.38	0.57
M418	0.34	0.24	0.30	0.31	-0.75	0.12	0.65
M067	0.35	0.31	0.02	-0.32	0.70	-0.14	-0.72
M426	0.65	0.61	0.61	-0.40	0.09	-0.60	-0.31
M138	0.40	0.47	0.45	-0.39	0.04	-0.60	0.01
M539	0.74	0.75	0.53	-0.76	0.73	-0.53	-0.71
M420	0.10	0.02	-0.15	0.10	0.11	0.01	-0.34
M427	0.81	0.75	0.60	-0.26	-0.35	0.07	0.14
BM2							
M414	-0.56	-0.50	-0.27	0.53	-0.80	0.23	0.75
M424	-0.86	-0.89	-0.90	0.82	-0.43	0.78	0.42
M141	0.33	0.30	0.11	-0.16	0.37	-0.31	-0.35
M430	0.44	0.41	0.15	-0.42	0.46	-0.33	-0.47
M417	0.60	0.55	0.32	-0.47	0.71	-0.38	-0.73
M429	-0.60	-0.58	-0.61	0.53	-0.26	0.42	0.39
UM1							
M583	-0.81	-0.84	-0.89	0.76	-0.39	0.70	0.41
M410	-0.68	-0.74	-0.85	0.71	-0.34	0.58	0.28
M538	-0.89	-0.88	-0.77	0.80	-0.61	0.71	0.65
M222	-0.87	-0.85	-0.75	0.77	-0.63	0.65	0.63
UM2							
M050	-0.77	-0.77	-0.59	0.79	-0.82	0.51	0.70
M217	-0.71	-0.71	-0.49	0.76	-0.85	0.42	0.76
M045	-0.83	-0.81	-0.67	0.75	-0.71	0.59	0.70

Fig. 4 Rainfall, ENSO, and large-scale climate quantile perturbation analysis results: all seasons. **a** UM1, UM2, and BM2 northeast aspect; **b** BM1 northeast; **c** BM1 and BM2 south aspect; and **d** other. All perturbation factors are in percent
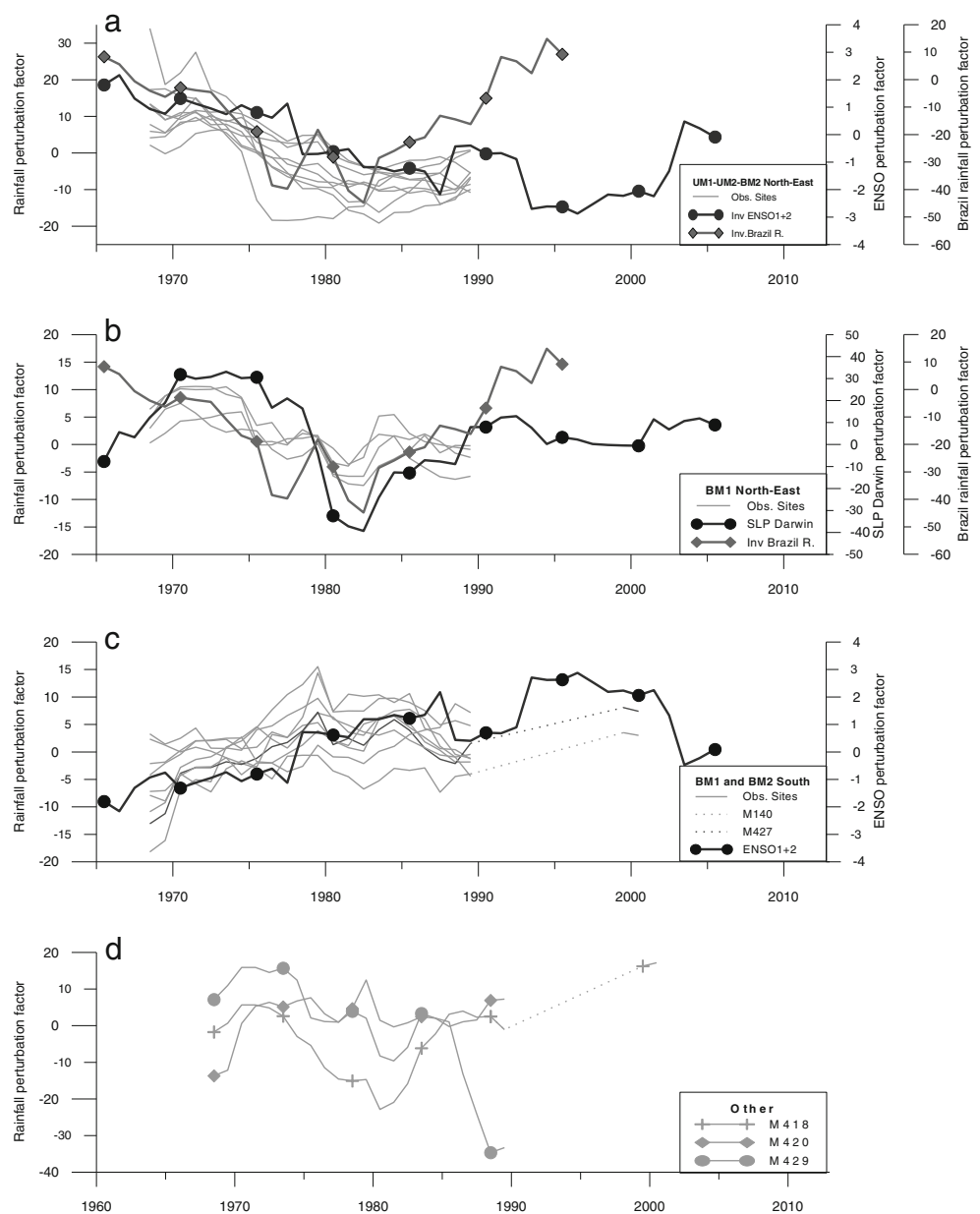
2000 and low anomalies during 1965–1974 and in the beginning of the 1990s (Fig. 4c), driven mainly by positive influence of ENSO. A third group of stations (M420, M418, and M429) shows a different pattern of anomalies with oscillation highs and lows occurring in a more random way in time and with no significant correlation with the large-scale climate influences (Fig. 4d).

The significance test showed that for the first group, the high and low anomalies of 1969–1974 and 1983–1986 are significant (at the 5% significance level) for the stations located in the regions UM1, UM2, and BM2 with northeast orientation. The high rainfall anomaly during 1969–1974 is significant for the sites in region BM1 with northeast orientation. The anomalies for the second group of stations with a southwest aspect are beyond the ranges of the 95%

confidence intervals for the high rainfall anomalies during 1978–1981 for nearly all the stations in that group. Less significant values are found for the low rainfall period of 1965–1974 for sites in the region BM2 with southwest orientation. The significance test applied to the last group of stations showed that the low rainfall period of 1983–1986 (based on the first group of stations) is highly significant for the stations M418 and M429.

The stations with medium and strong Amazon regime (UM1 and UM2) in the eastern part of the basin, together with the sites located in the mountain region BM2 with a northeast aspect, are negatively correlated to the SST ENSO 1.2. The correlation factors for UM1 and UM2 are $R^2=0.67$ and $R^2=0.60$, respectively, and $R^2=0.53$ for BM2. Also a negative correlation with Brazil rainfall is found.

Fig. 5 Correlation between anomalies of observed sites and anomalies of different large-scale climate influences for temperature and rainfall in all seasons
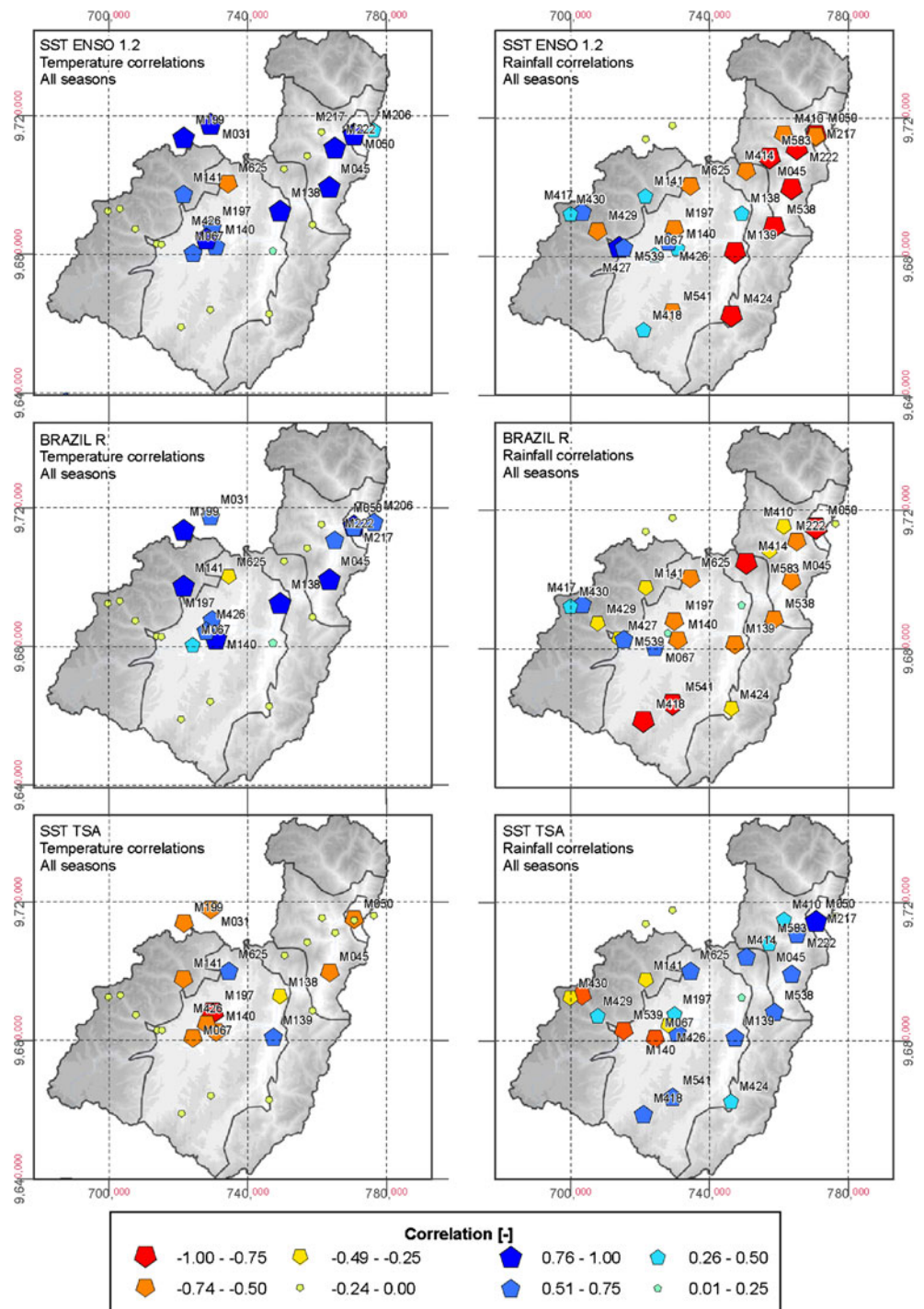
Stations with a northeast aspect in regime BM1 are correlated with SLP Darwin–Tahiti and negatively correlated with the Brazil rainfall with $R^2=0.57$ and $R^2=0.48$, respectively. Stations with a southwest orientation are positively correlated with the SST ENSO 1.2 for BM1 ($R^2=0.35$) and for BM2 ($R^2=0.22$).

Plotting these different groups (Fig. 5), it can be observed that the eastern part of the basin is negatively correlated with the SST ENSO1.2 and with the Brazil rainfall and positively correlated with the SST TSA. In the inter-Andean valley regions and western sites, this influence depends on the terrain orientation (aspect). In summary, it can be concluded that the annual anomalies in the regions UM1, UM2, and BM2 with northeast aspect are strongly negatively correlated with the SST ENSO and negatively correlated with the Brazil rainfall. Region BM1

with northeast aspect shows an inverse influence of the ENSO but has a stronger negative correlation with the Amazon rainfall. Regions BM1 and BM2 with south aspect are positively correlated with the SST ENSO1.2 but in a less significant way.

3.2 Anomalies for specific seasons

The same analysis has been repeated for 3-month periods to estimate anomaly patterns in different seasons of the year.

3.2.1 Temperature

Results on the anomalies for specific seasons present similar results when compared to the results for all seasons. This means low-temperature anomalies during the years 1969–1973 and high anomalies during 1979–1984, which are mainly influenced by ENSO (Fig. 6). The correlations, however, are stronger/weaker for specific seasons. As in the case of all seasons, the anomaly values and the significance of anomalies are higher at high elevation sites. For the period of DJF (Fig. 6a), 11 of the 16 stations show high correlation with the SST ENSO 1.2 and ENSO 3 (R^2=0.79 and 0.78, respectively). During this season, the sites that are located at higher elevations show more significant anomaly values than in the analysis for all seasons. The sites that are located in the deep inter-Andean valley region show lower anomaly values when compared with the analysis for all seasons.

For the season of MAM, similar results as for the season DJF are obtained in 13 of the 16 stations but with lower correlation values. These anomalies are positively correlated to the SST ENSO 3 and the Brazil rainfall (R^2=0.77 and 0.63, respectively). Low-temperature anomalies are found during the years 1969–1973 and high anomalies during 1979–1984 (see Fig. 6b). When compared with the anomalies for all seasons, more extreme and significant anomalies are found. The strong correlation that the ENSO has in the period of DJF is still present in the period of MAM. The Paute River Basin and the Brazil rainfall are, however, positively correlated in the period of MAM.

During the period of JJA, 10 of the 16 stations show anomaly patterns with lower temperatures during the years 1964–1974 (with a minimum on 1971) and higher values during 1978–1986 (with a maximum on 1984; see Fig. 6c). These anomalies are negatively correlated with the Eastern Pacific Oscillation (R^2=0.65) but less correlated with the ENSO 1.2 oscillation as in the previous periods (R^2=0.52). These low correlations might imply that local influences could play a larger role than the ENSO during this period. For the station sites M032 and M625, the anomaly is different, which could involve other external or local influences. There is a need to further investigate possible

sources of climatic influences in the region, especially for this period when the ENSO influence is weak. The anomalies are high and significant during JJA, similar to the period of DJF, despite the fact that the influence of ENSO is weak.

For the period of SON, 10 of the 16 sites show similar results as the season of DJF. Low-temperature anomalies are found during the period 1968–1974 (with a minimum on 1971) and high anomalies in the period 1979–1984 (with a maximum on 1982). The anomaly values can differ between stations, showing higher and significant anomaly values for the higher elevation sites. The values are, however, less extreme when compared with other seasons. The anomalies have high correlation with the SST ENSO 3 and ENSO 1.2 (R^2=0.65 for both).

3.2.2 Rainfall

In the all-season analysis, the stations were grouped according to the hydrological regime and orientation (aspect). This resulted in the following groups: (a) eastern part of the basin and some inter-Andean valley sites with northeast aspect and (b) some inter-Andean valleys and western sites with southwest aspect. The same analysis is repeated here but based on the 3-month periods.

The negative correlation with SST ENSO1.2 and Brazil rainfall and the positive correlation with the SST TSA found for the first group of stations are stronger for the season of SON. This means high rainfall anomalies during 1969–1973 and 1986–1988 and low rainfall anomalies during 1979–1984. However, negative correlation was also found for stations that belong to regimes UM1 and UM2 with the SST EPO ($R2$=0.69 and $R2$=0.44, respectively). The stations from the regimes BM2 and BM1 with a northeast orientation are also negatively correlated, but in a lower way, with the SST EPO ($R2$=0.60).

The positive correlation with the SST ENSO1.2 in some of the inter-Andean valley regions and western sites is stronger in the season MAM (see Fig. 7), especially in stations with south or southeast aspect. They show a negative rainfall anomaly during 1965–1973 and a positive rainfall anomaly during 1979–1985. The anomaly values of this group present a direct correlation with the SST ENSO 3 and SST ENSO 1.2 ($R2$=0.61 and 0.56, respectively).

In the period of MAM, another group of stations with north or northeast aspect shows high anomalies during 1970–1974 and low anomalies during 1985–1990. This group presents a negative correlation with the SST ENSO 3 and SST ENSO 1.2 ($R2$=0.54 and 0.58, respectively).

For the period of DJF, no clear influence of the climate external influences is shown. This indicates that the high negative correlations found for the all seasons anomalies
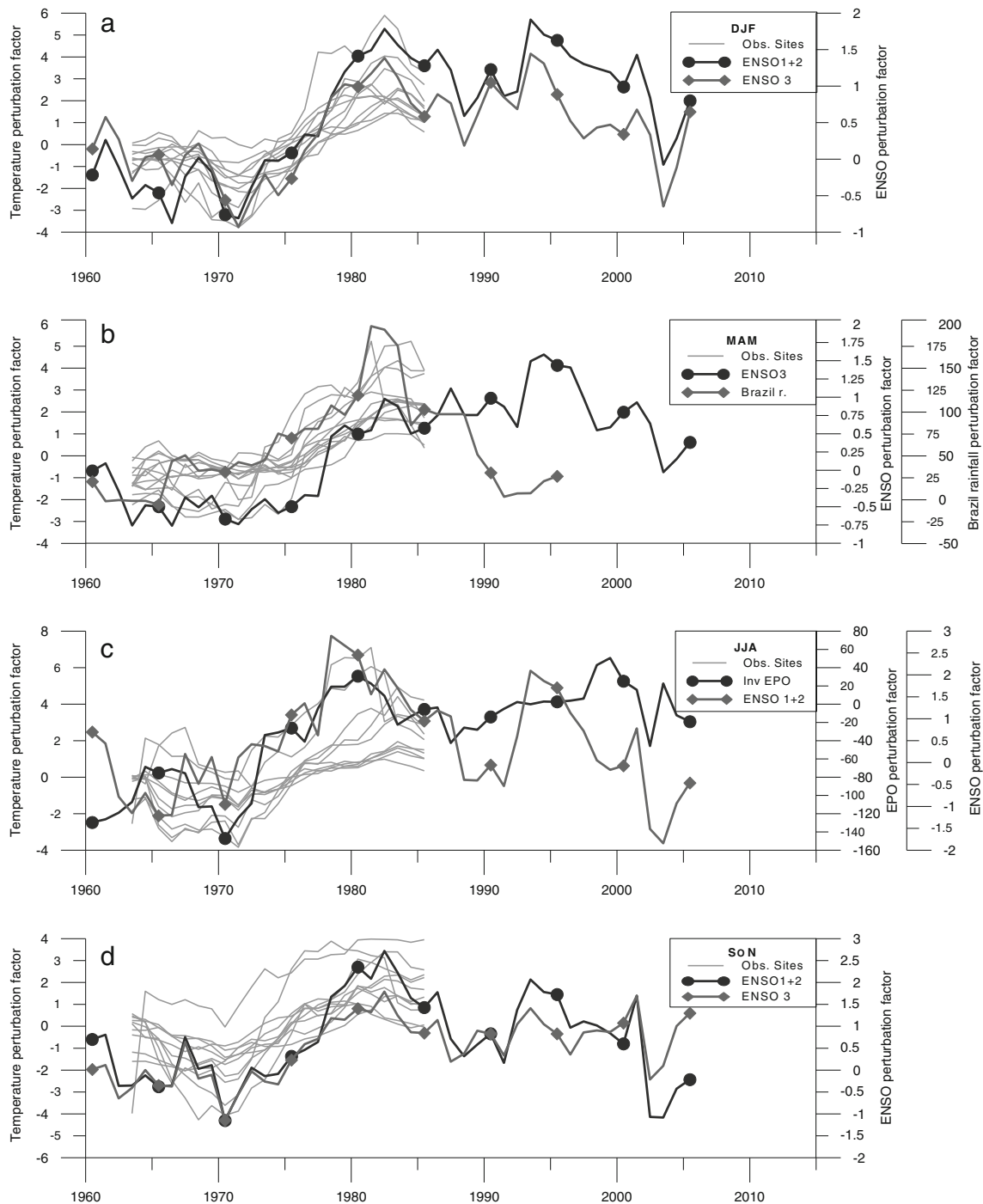
Fig. 6 Temperature and large-scale climate quantile perturbation analysis results for individual seasons. **a** DJF, **b** MAM, **c** JJA, and **d**. SON. All perturbation factors are in percent

with ENSO, for most of the stations, are due to rainfall in other periods of the year. Grouping of the stations by regime and/or aspect did not alter these results. This lack of correlation might be caused by the transition of external influences for SON and MAM. However, in DJF, two groups of stations were identified. Stations M197, M067, M140, M414, and M045 have high correlation with the tropical

Pacific anomaly (R^2=0.58). The anomalies are high during the periods 1968–1974 and 1984–1986 and low during 1980–1983. Another group of stations involves the stations corresponding to the UM2 regime, but these do not show a large-scale climate influence. They have high anomalies during 1969–1974 and 1986–1989 and low anomalies during 1976–1979. The anomaly values do not depend on the
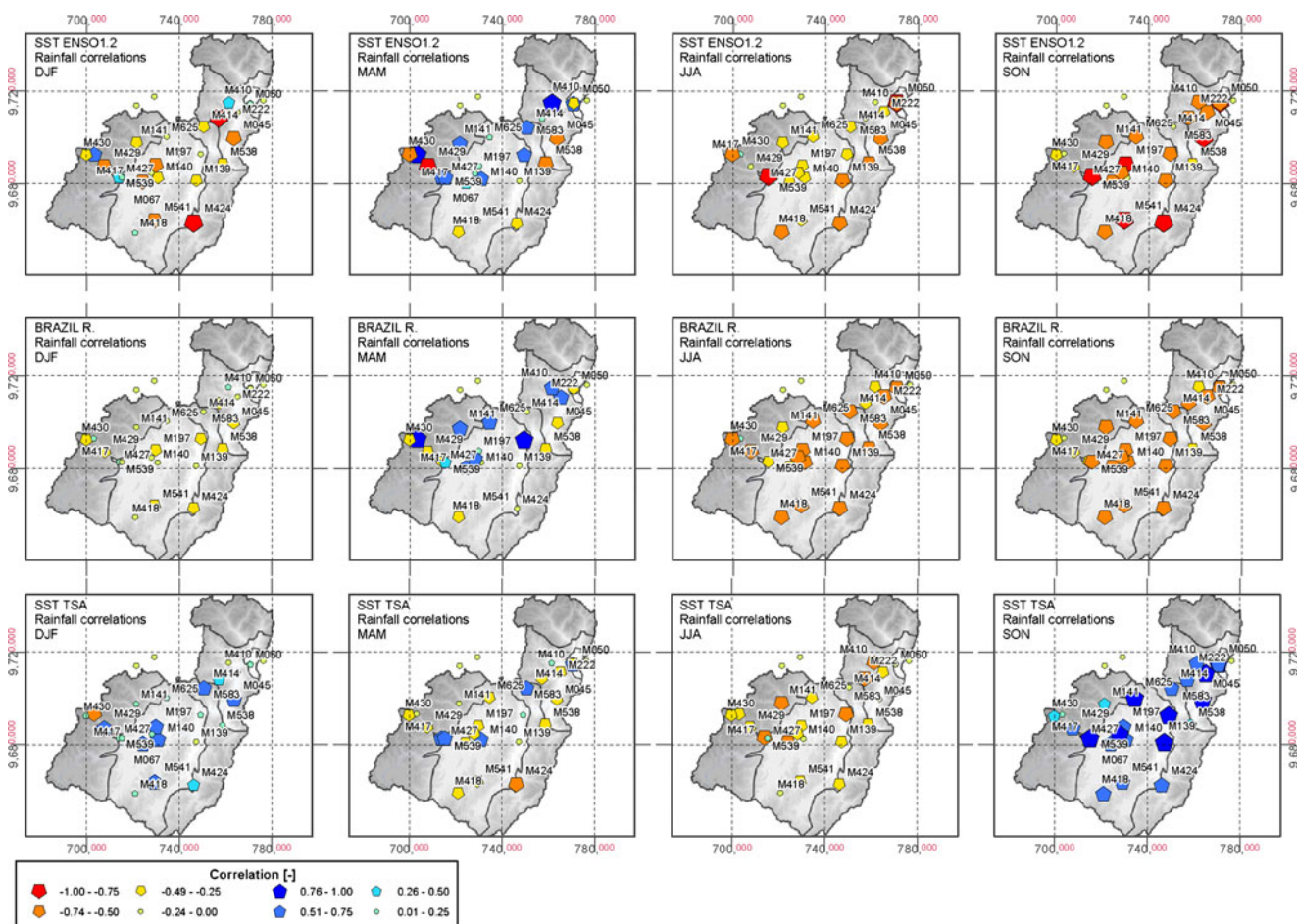
Fig. 7 Correlation between anomalies of observed sites and anomalies of different large-scale climate influences for rainfall in different seasons

hydrological regime or the aspect, with the exception of UM2.

For the period of JJA, the 25 stations show similar oscillations, with high anomalies during 1968–1976 and low anomalies during 1981–1989. These anomaly values have a negative correlation with the SST ENSO 3 and a positive correlation with the SST EPO (R^2=0.59 and 0.63, respectively). When the negative correlation with the SST ENSO 3 is studied separately per rainfall regime, R^2 values of 0.53, 0.41, 0.54, and 0.52 are found for the BM1, BM2, UM1, and UM2 regions, respectively. The period of JJA shows the same behavior than the period of SON but with lower correlations for the SST ENSO1.2 and Brazil rainfall. The influence of the SST TSA is lower during this period and shows negative correlation.

From the rainfall, results we learn that the region is partially influenced by ENSO as was suggested by Marengo (2009), but only in few regions, especially in the western part of the basin. Results, however, also suggest that the ENSO is not the unique driver that influences the region and that other factors might be present. This result is similar to the one found by Bendix and Bendix (2006).

These authors explain that Amazon rainfalls might cross the Andes and even influence the coastal region. The results show similarities with the investigation by Vuille et al. (2000), which concluded that the Eastern Cordillera (eastern part of the River Paute Basin) is correlated to the SST TSA and that few local areas are correlated with the ENSO. Positive correlation with the ENSO in the western part of the basin confirms the studies by Rodbell et al. (1999) who found the influence of ENSO on paleorecords in Laguna Pallacocha and Francou et al. (2004) who found the ENSO influence on the Antisana. However, differences are found in the dominant period of ENSO influence in the Andes. Vuille et al. (2000) found that the most dominant period is DJF, while in this research the results show that ENSO influence in precipitation is stronger in MAM.

4 Conclusions

The analysis of the decadal oscillations in anomalies of rainfall and temperature has shown that historical variations in rainfall and temperature for the stations in the Paute

River Basin differ depending on elevation, hydrological regime, and orientation (aspect). Historical variations in temperature, when considering all seasons combined, show strong similarities in the results across the basin. Most of the sites show lower temperatures during 1968–1973 and a warmer period during 1978–1984. The significance of the anomalies in temperature is higher at sites with higher elevations. They are highly correlated with the SST ENSO 1.2 and ENSO 3. For the deep inter-Andean valley stations, anomalies and their correlation with the ENSO are less significant. During the months DJF, most of the stations show a stronger correlation with the SST ENSO 1.2. For the other seasons, the influence of ENSO is also present, but less strong. The ENSO influence is lower for the season of JJA. This supports a better understanding of the influence of ENSO on temperature along the Paute River Basin.

The historical variations in rainfall are diverse. Results show that for the eastern stations (Amazon regime), anomaly values are more significant. High anomaly values are found during 1969–1974 and low values during 1983–1986, which are negatively correlated with the SST ENSO 1.2. For the other stations, the anomalies behave in a more random way in time (less similarity between stations: high and low anomaly values in different periods). Also the significance of these anomalies and their correlation with the large-scale climate influences is less clear. The stations from the BM2 region (high mountain regime) with a northeast aspect show strong anomalies (high rainfall during 1969–1974 and low rainfall during 1983–1986) similar to the regions UM1 and UM2. The inter-Andean valley stations, located in the region BM1 with northeast aspect, show similar behavior as UM1 and UM2 too, but with less significant values and lower correlation to large-scale climate influences. The stations with southwest aspect, for the regions BM1 and BM2, match in their anomalies: A high rainfall period during 1978–1981 and a low rainfall period during 1965–1974 but less significant than for the other sites and their correlations with the large-scale climatic influences are less clear. The season SON shows stronger negative correlations with the SST ENSO 1.2, Brazil rainfall, and stronger positive correlation with the SST TSA for the stations located in the UM1 and UM2 regions and the BM1 and BM2 regions with northeast aspect. Meanwhile, the season of MAM shows positive correlation with the SST ENSO1.2 for some western stations.

This study has given more insight in the climate variability at local scale in the Paute River Basin of the Ecuadorian Southern Andes, after identifying similarities and differences in temporal patterns of temperature and rainfall along the basin. The correlations with climate external influences are simpler for temperature series and more complex for rainfall series. Given that much larger records are available for the climate external influences

than for the rainfall and temperature series, these correlations might help to extrapolate the patterns of temperature and rainfall beyond the observation periods.

The quantile perturbation method would also be useful to estimate trends in climate values. However, the usefulness strongly depends on the length of the available data series. In this research, the data series length was limited to 30 years, which is not enough to find several complete oscillation cycles to estimate the significance of recent trends. The data for the more recent years (after the 1990s) were, moreover, unluckily unavailable, except for the three stations mentioned, which have similar trends as their most correlated climate variables. The present research therefore has been limited to the identification of decadal oscillations. The results in this research approach the results in Marengo (2009), in which the Amazon rainfall indicates long-term variations of decadal and multi-decadal modes rather than any unidirectional trend toward drier or wetter conditions. These new insights clearly help in separating trends from natural variability in future research activities.

References

Bendix A, Bendix J (2006) Heavy rainfall episodes in Ecuador during El Nino events and associated regional atmospheric circulation and SST patterns. Adv Geosci 6:43–49

Buytaert W, Vuille M, Dewulf A, Urrutia R, Karmalkar A, Celleri R (2010) Uncertainties in climate change projections and regional downscaling in the tropical Andes: implications for water resources management. Hydrology and Earth System Sciences 14:1247–1258

Carter RW, Benson MA (1970) Concepts for the design of a streamflow data program. Open-file report, U.S. Geological Survey, 20 p

Celleri R, Willems P, Buytaert W, Feyen J (2007) Space–time variability of rainfall in the Paute River Basin of South Ecuador. Hydrol Process 21:3316–3327

Coltorti M, Ollier CD (2000) Geomorphic and tectonic evolution of the Ecuadorian Andes. Geomorphology 32:1–19

Francou B, Vuille M, Favier V, Cáceres B (2004) New evidence for an ENSO impact on low-latitude glaciers: Antizana 15, Andes of Ecuador, 0°28′ S. J Geophys Res 109:D18106

Galarraga-Sanchez, R., 2000. Informe Nacional sobre la gestion del agua en el Ecuador. Comite Asesor Tecnico de America del Sur (SAMTAC). Global Water Partnership (GWP), Quito-Ecuador February 2000, 80p. http://www.unesco.org.uy/phi/vision2025/Ecuador.pdf

Le Goulven P, Ruf T, Ribadeneira H (1987) Presentación del Proyecto INERHI (Instituto Ecuatoriano de Recursos Hidraulicos,

Ecuador)—ORSTOM (Office de la Recherche Scientifique et Technique d'Outre-Mer, France). Quito, Ecuador 1987:23p

Makhuvha T, Pegram G, Sparks R, Zucchini W (1997) Patching rainfall data using regression methods I. Best subset selection, EM and pseudo-EM methods: theory. J Hydrol 198:289–307

Marengo JA (2009) Long-term trends and cycles in the hydrometeorology of the Amazon basin since the late 1920s. Hydrol Process 23:3236–3244

Ntegeka V, Willems P (2008) Trends and multidecadal oscillations in rainfall extremes, based on a more than 100-year time series of 10 min rainfall intensities at Uccle, Belgium. Water Resources Research 44. doi:10.1029/2007WR006471

Ontaneda G, García G, Arteaga A (2002) Evidencias del Cambio Climático en Ecuador. Actualización. Comité Nacional sobre el Clima GEF-PNUD. Ministerio del Ambiente. Proyecto ECU/99/G31 Cambio Climático-Fase II, Quito, Ecuador, 92 p

Parry ML, Canziani OF, Palutikof JP, Van der Linden PJ, Hanson CE (2007) Contribution of Working Group II to the Fourth Assessment Report of the Intergovernmental Panel on Climate Change. Cambridge University Press, Cambridge, 976 pp

Rodbell DT, Seltzer GO, Anderson DM, Abbot MB, Enfield DB, Newman JH (1999) An approximately 15,0000-year record of El Nino-driven alleviation in southwestern Ecuador. Science 283 (5401):516–520

Solomon S, Qin D, Manning M, Chen Z, Maqruis M, Averyt KB, Tignor M, Miller HL (2007) Contribution Working Group I to the Fourth Assessment Report of the Intergovernmental Panel on Climate Change. Cambridge University Press, Cambridge, 996 p

Torrence C, Webster PJ (1999) Interdecadal changes in the ENSO-monsoon system. J Clim 12:2679–2690

Torres P (2004) Correlación como herramienta para analizar la distribución de precipitación en la cuenca del rio Paute. M.Sc. thesis, Programa para el Manejo del Agua y del Suelo, Universidad de Cuenca, Cuenca, Ecuador, 80 p

Villar JC, Roncahil J, Guyot JL, Cochonneau G, Naziano F, Lavado W, De Oliveira E, Pombosa R, Vauchel P (2009) Spatio-temporal rainfall variability in the Amazon basin countries (Brazil, Peru, Bolivia, Colombia and Ecuador). Int J Climatol 29:1574–1594

Villazon MF, Willems P (2010) Filling gaps and daily disaccumulation of precipitation data rainfall–runoff model. Proceeding in the Fourth International Scientific Conference BALWOI 2010 on water observation and information systems for decision support, Rep. Macedonia, 25–29 May 2010

Vuille M, Bradley RS, Keiming F (2000) Climate variability in the Andes of Ecuador and its relation to tropical Pacific and Atlantic sea surface temperature anomalies. J Clim 13:2520–2535

Vuille M, Francou B, Wagnon P, Juen I, Kaser G, Mark BG, Bradley RS (2008) Climate change and tropical Andean glaciers: past, present and future. Earth-Science Reviews 89:79–96

Wang C, Fiedler PC (2006) ENSO variability and the eastern tropical Pacific: a review. Progress In Oceanography 69:239–266